Mechanisms in non-heme iron oxidation catalysis

Chen, Juan

CHAPTER 3

A non-heme iron photocatalyst for light driven aerobic oxidation of methanol

The non-heme (L)Fe^{III} and (L)Fe^{III}-O-Fe^{III}(L) complexes (L = 1,1-di(pyridin-2-yl)-N,N-bis(pyridin-2-ylmethyl)ethan-1-amine) undergo reduction under irradiation to the Fe^{II} state with concomitant oxidation of methanol to methanal, without the need for a secondary photosensitizer. Spectroscopic and Density Functional Theory (DFT) studies support a mechanism in which irradiation results in charge transfer excitation of a Fe^{III}-μ-O-Fe^{III} complex to generate $[(L)Fe^{IV}=O]^{2+}$ (observed transiently during irradiation in acetonitrile), and an equivalent of (L)Fe^{II}. Under aerobic conditions, irradiation accelerates reoxidation from the Fe^{II} to Fe^{III} state with O_2 closing the cycle of methanol oxidation to methanal.

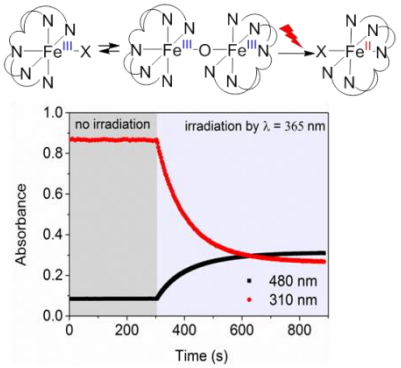

This chapter has been published:

Juan Chen, Stepan Stepanovic, Apparao Draksharapu, Maja Gruden, and Wesley R. Browne, *Angew. Chemie Int. Ed.* 10.1002/anie.201712678.

3.1 Introduction

Photoredox catalysis has emerged as a versatile method to access highly reactive species in a selective and clean manner.[1,2] The redox-active photosensitizers available include organic dyes,[3] inorganic clusters,[4] and transition metal complexes, such as $[Ru(bpy)_3]^{2+}$ and its derivatives,[5,6] whose redox potentials can be fine-tuned by ligand modification.[7–9] Photoredox catalysis can bypass reactive stoichiometric oxidants, *e.g.*, H_2O_2, ClO^-, etc. to generate high-valent transition metal oxido species by electron transfer oxidation. Recently, non-heme iron complexes that are well-known catalysts for a wide range of oxidations were combined with photoredox catalysts, such as $[Ru(bpy)_3]^{2+}$, for light driven oxidations.[9–11] In this multi-catalyst strategy (**Scheme 5**) excitation of the photoredox sensitizer is followed by electron transfer oxidation of the catalyst to raise it to a higher oxidation state and subsequently oxidize substrates. The photoredox sensitizer is reoxidised by an electron acceptor (EA), however, the use of atom-economic terminal oxidants (*e.g.*, O_2) is a key challenge and it would be preferable to use a single catalyst that is driven directly by light through the entire redox cycle. In addition, the generation of other species such as singlet oxygen by the organic and Ru(II)/Ir(III) photosensitizers is difficult to avoid.[12–17]

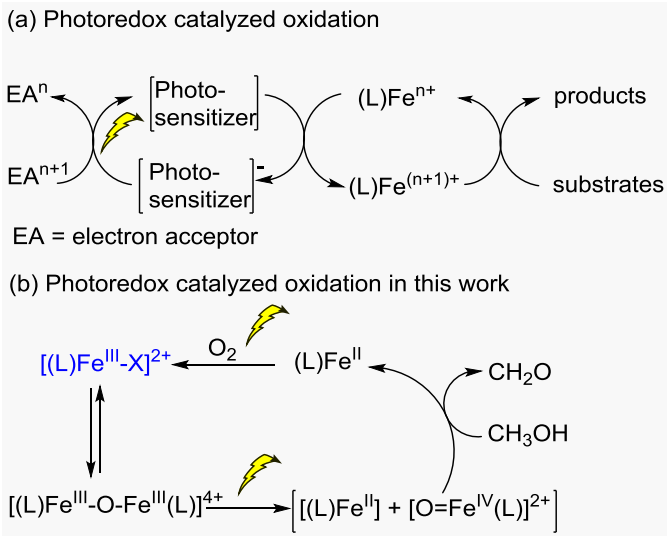

Scheme 5. (a) Multi-catalyst strategy for photocatalytic reaction, and (b) single catalyst photocatalytic oxidation described herein. Where L = MeN4Py, X = OMe or Cl.

The photochemistry of iron complexes and especially the reduction of complexes from the Fe^{III} to the Fe^{II} state when irradiated is well established,[18] not least in the widely used chemical actinometer $[Fe^{III}(oxalato)_3]^{3-}$,[19] and other iron(III) carboxylato complexes.[20] Photoreduction in such systems is irreversible and accompanied by ligand oxidation (*e.g.,* CO_2 formation from carboxylate ligands) and hence Fe^{III} complexes are of limited use in the photocatalytic oxidation of organic substrates. Notable exceptions (vide infra) are to be found in the reports of Richman,[21,22] Karlin[23] and co-workers in the 1980s on the photochemistry of μ-oxido bridged diiron(III) complexes.

Previously, we reported that non-heme Fe^{II} complexes (such as $[(MeN4Py)Fe^{II}(CH_3CN)]^{2+}$ **1**, **Figure 40**) are photoinert in acetonitrile, but undergo light-driven oxidation (from the Fe^{II} to Fe^{III} redox state) with O_2 in solvents in which the CH_3CN ligand is displaced by the solvent used.[24] The photochemically driven oxidation of an Fe^{II} complex together with the earlier reports of photoreduction of Fe^{III} complexes raises the possibility that a fully light driven photocatalytic

oxidation cycle can be achieved without a separate photosensitizer such as $[Ru(bpy)_3]^{2+}$ (**Scheme 5**). However, simple non-heme Fe^{III} systems lack the distinct photophysics and chromophoric properties of the heme unit present in the systems of Richman,[21,22] Karlin[23] and co-workers, and hence it would seem unlikely that a fully non-heme Fe^{III} complex would show similar photoreactivity.

Here, we show that a single iron-based catalyst can promote catalytic oxidation reactions without the use of a secondary photosensitizer (**Scheme 5b**). We report the light-driven double photocycle capable of high-turnover oxidation of methanol with O_2 as terminal oxidant. Photoreduction of the non-heme iron(III) complexes to the Fe^{II} state occurs concomitant with the oxidation of methanol and is followed by light-driven reoxidation of the iron(II) complex, with O_2 as terminal oxidant (**Scheme 5b**). The whole cycle proceeds without significant ligand degradation.

Density functional (DFT) methods support the assignment of the μ-oxido diiron(III) complex **2a** (**Figure 40**) as the photochemically reactive species with photoreduction proceeding via a $[(L)Fe^{IV}=O]^{2+}$ intermediate analogous to that reported for the heme-based systems.[21–23] $[(L)Fe^{IV}=O]^{2+}$ (**4**) is itself photoreactive, as we have shown recently.[25] However, under certain conditions this species can also be observed during the irradiation of **2a** in acetonitrile. The formation of $[(L)Fe^{IV}(O)]^{2+}$ (**4**) during irradiation opens the possibility for selective photocatalytic oxidation reactions.

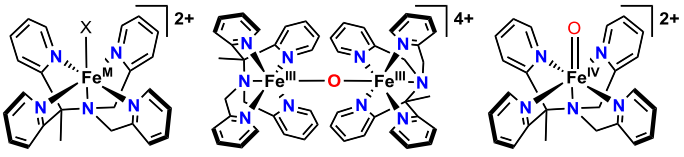

Figure 40. Structures of complexes **1-4** used in this work.

3.2 Results and Discussion

Irradiation of the Fe^{III} complexes $[(L)Fe^{III}(OCH_3)]^{2+}$ (**2**) and $[(L)Fe^{III}(Cl)]^{2+}$ (**3**) in argon-purged methanol at 365 nm resulted in a decrease in absorbance at 310 nm and concomitant increase in absorbance at 380 and 480 nm corresponding to formation of Fe^{II} complexes (**Figure 41** and **Figure 42**). Irradiation of **3** at 300 nm resulted in similar changes, however, there was a pronounced wavelength dependence of photochemical quantum yield[26,27] ($\Phi_{300\ nm}$ = 0.31 ± 0.01, $\Phi_{365\ or\ 355\ nm}$ = 0.07 ± 0.01). Irradiation at 490 nm does not affect the absorption spectrum (**Figure 43**) even though this wavelength is in resonance with a weak absorption band. Changes in absorbance were not observed without irradiation (**Figure 41** and **Figure 44**). Essentially identical changes were observed upon irradiation of **2a** in methanol at 365 nm as with **2** and **3** (**Figure 45**). The identical behavior of all three complexes in argon-purged methanol reflects the rapid equilibration of **2a** and **3** with methanol to form predominantly **2**, as confirmed by resonance Raman (λ_{exc} 355 nm, **Figure 46**) spectroscopy.

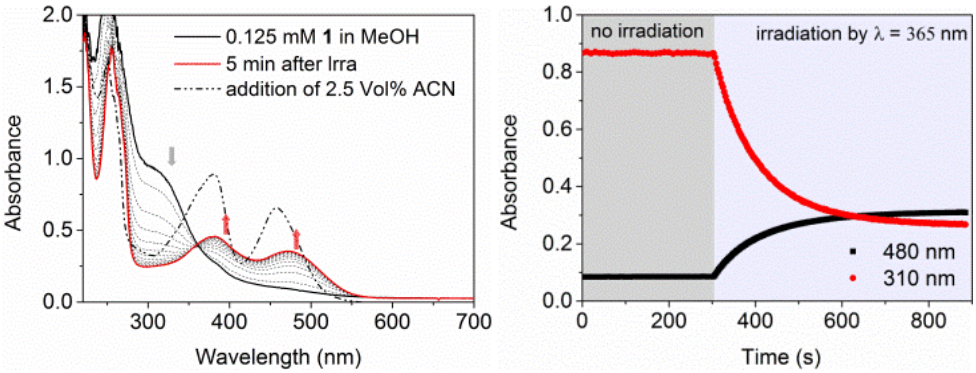

Figure 41. (Left) UV-vis absorption spectrum of **3** (0.125 mM, black solid line) in deoxygenated methanol, during (dotted lines) and after (red solid line) irradiation at 365 nm, and after subsequent addition of 2.5 vol % acetonitrile (black dash-dotted line). (Right) Absorbance at 310 and 480 nm over time in the dark and under irradiation.

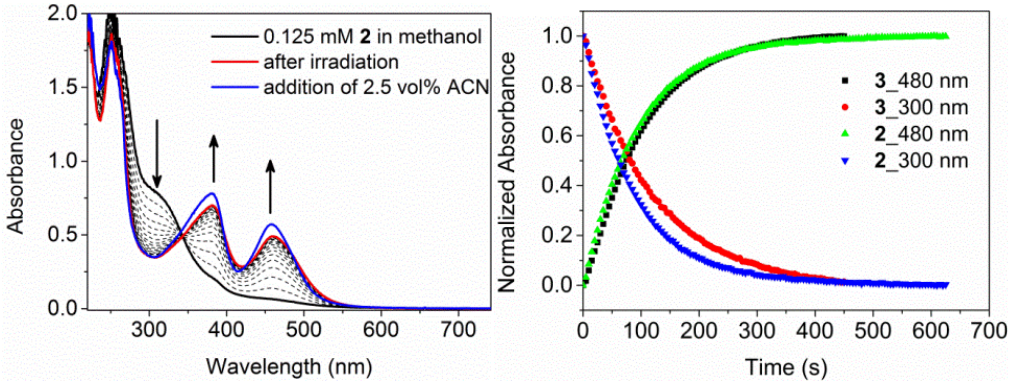

Figure 42. (Left) UV-vis absorption spectrum of **2** (0.125 mM, black solid line) in argon-purged methanol, during (dotted lines) and after (red solid line) irradiation at 365 nm, and after subsequent addition of 2.5 vol % acetonitrile (blue solid line). (Right) Absorbance changes at 300 and 480 nm of **2** and **3** (0.125 mM) in deoxygenated methanol over time under irradiation (λ_{exc} 365 nm). The absorbance at 300 nm is normalized at t = 0 s and at 480 nm at t = 600 s.

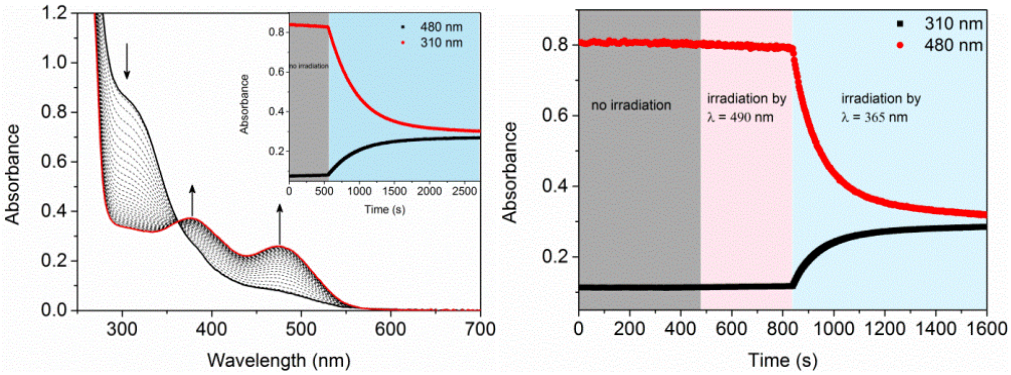

Figure 43. (left) UV-vis absorption spectrum of **3** in deoxygenated methanol (black solid line) under irradiation at 300 nm (inset shows the absorbance at 310 and 480 nm with time). (Right) Absorbance at 310 and 480 nm over time with initially no irradiation, irradiation at 490 nm and at 365 nm.

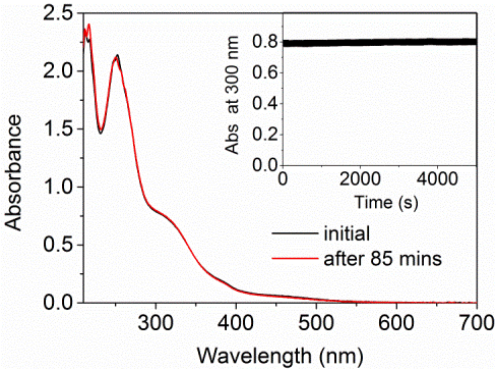

Figure 44. UV-vis absorption spectrum of **2** (0.125 mM) in deoxygenated methanol at 0 and 85 min without irradiation. Inset shows the absorbance at 300 nm over time.

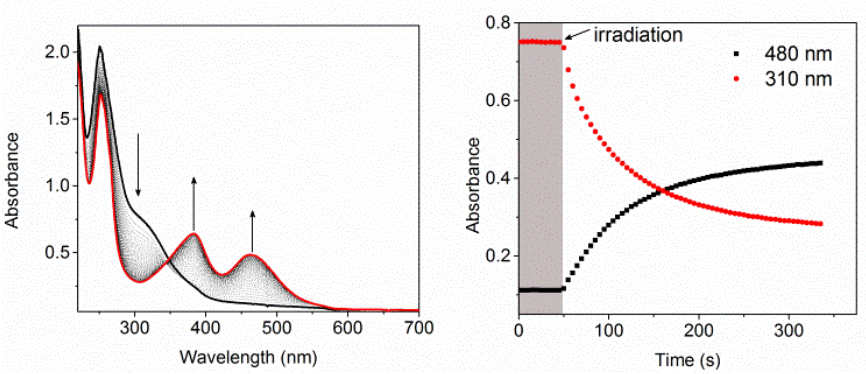

Figure 45. (Left) UV-vis absorption spectrum of **2a** (0.0625 mM) in deoxygenated methanol under irradiation at 365 nm. (Right) Absorbance at 310 and 480 nm over time in the dark and under irradiation.

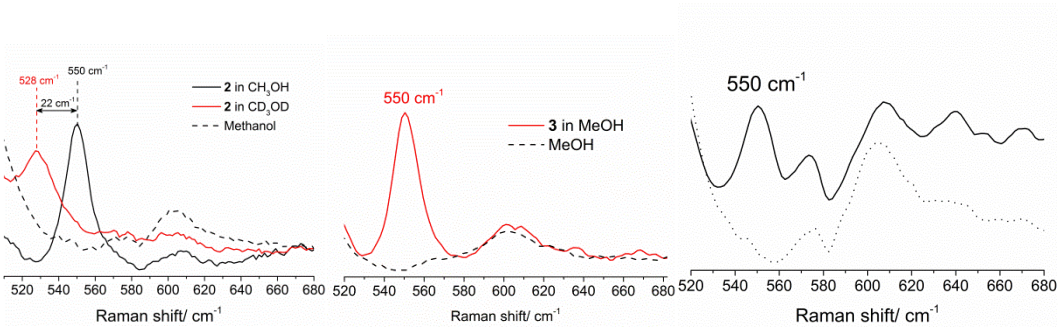

Figure 46. Resonance Raman (λ_{exc} 355 nm) spectrum of **2** (left), **3** (middle) and **2a** (right) in methanol; the band at 550 cm^{-1} was assigned to Fe-O stretching mode in $[(MeN4Py)Fe^{III}\text{-}OMe]^{2+}$ by comparison of the spectrum in CH_3OH and CD_3OD (with CH_3OD there is no isotopically induced shift of the 550 cm^{-1} band).

Addition of acetonitrile (to 2.5 vol%) after irradiation confirmed the integrity of the ligands by yielding the corresponding $[(L)Fe^{II}(CH_3CN)]^{2+}$ complex (**1**) quantitatively; by comparison with the absorption spectrum of $[(L)Fe^{II}(CH_3CN)]^{2+}$ (**1**) in acetonitrile (**Figure 41** and **Figure 47**).[24,28] The concomitant formation of 0.5 equivalents of formaldehyde confirmed that methanol was the source of electrons for the reduction.

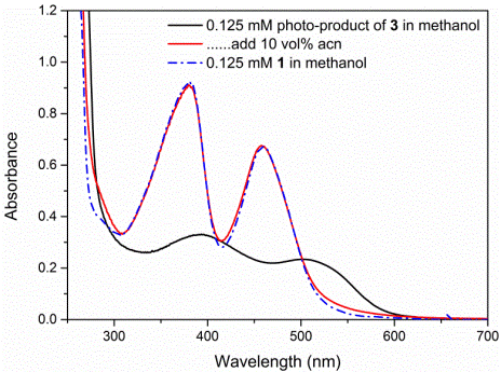

Figure 47. UV-vis absorption spectrum of the photo-product obtained upon irradiation of **3** in argon purged methanol at 365 nm (black solid line), after addition of 10 vol% of acetonitrile (red solid line); 0.125 mM $[(Men4py)Fe^{II}(CH_3CN)]^{2+}$ (**1**) in acetonitrile.

The dependence of the photochemistry on wavelength (see above) indicates that not all of the species (e.g., **2**, **2a**, etc.) present in solution are photoactive (see below). Although the expected S = ½ Fe^{III} (X-band) EPR signals of **2** were observed at 77 K (**Figure 48**), quantification indicates that in deoxygenated methanol, only 40% of the Fe^{III} is present as a mononuclear S = ½ Fe^{III}-OCH_3 complex. The remaining 60% is EPR silent, possibly present in the Fe^{III}-O-Fe^{III} form, *e.g.* **2a**, or as mononuclear complexes with coordination modes that lead to fast electron-spin relaxation (and hence EPR silence as observed for **3** in acetonitrile). Hence the UV-vis absorption spectrum of **2** (and **3**) in deoxygenated methanol and in acetonitrile is a weighted sum of the spectra of $[(L)Fe^{III}\text{-}OCH_3]^{2+}$ (**2**) (or $[(L)Fe^{III}\text{-}Cl]^{2+}$, **3**, **Figure 48**), $[(L)Fe^{III}\text{-}\mu\text{-}O\text{-}Fe^{III}(L)]^{2+}$ (**2a**) and other related species.[29]

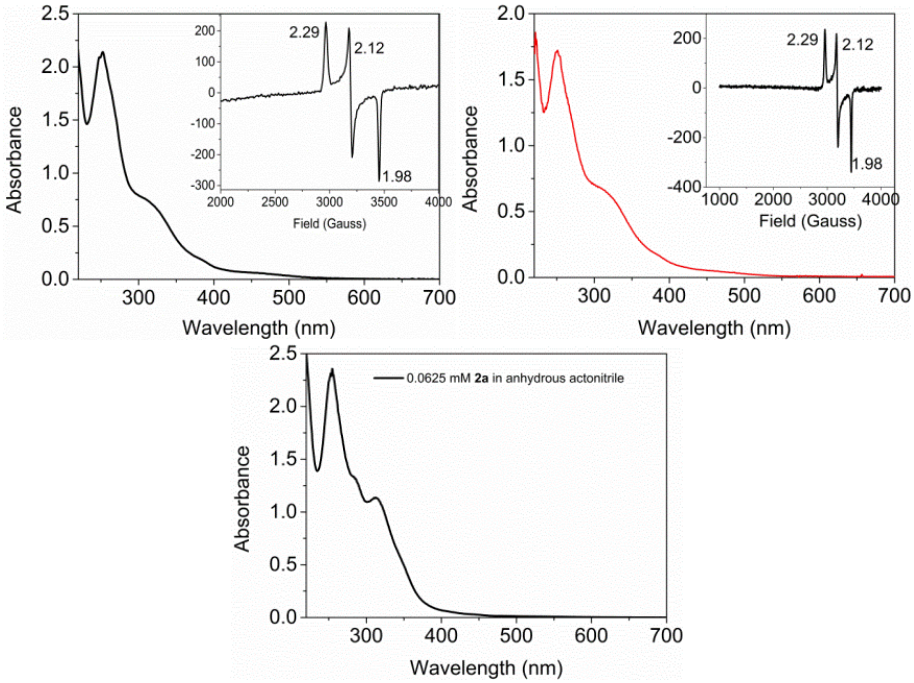

Figure 48. UV-vis absorption spectra of **2** (top left) and **3** (top right) in methanol; X-band EPR spectra at 77 K are shown as insets. (bottom) UV-vis spectra of **2a** (0.0625 mM) in anhydrous acetonitrile.

The addition of NaOAc (50 equiv) to **2** in argon-purged methanol resulted in slight but immediate change in its UV-vis absorption spectrum (**Figure 49**, and for **3** see **Figure 50**) but

thereafter no further thermally induced changes were observed. The rate of photoreduction was, however, increased fourfold (**Figure 49**). Again subsequent addition of acetonitrile (*see above*, **Figure 51**) in the quantitative formation of $[(L)Fe^{II}(CH_3CN)]^{2+}$ (**1**), thus confirming the integrity of the ligand (L).

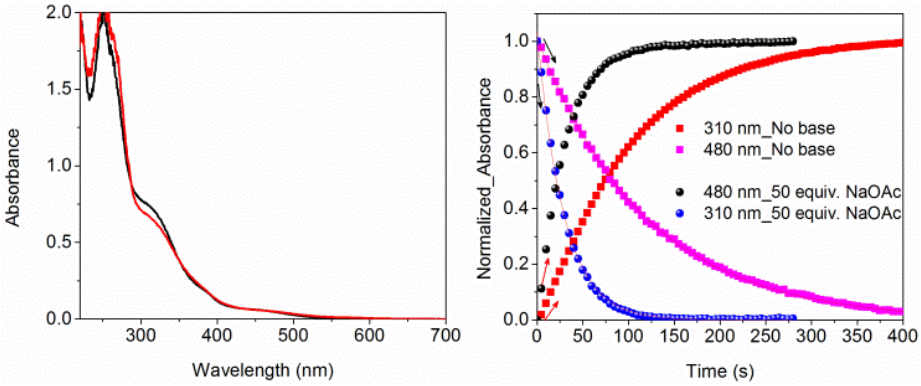

Figure 49. (left) UV-vis absorption spectrum of **2** in methanol (black) and after addition of NaOAc (50 equiv) (red); (Right) Comparison of normalized absorbance at 310 nm and 480 nm over time under irradiation (λ_{exc} 365 nm) with (black, blue) and without (red, pink) NaOAc (6.25 mM).

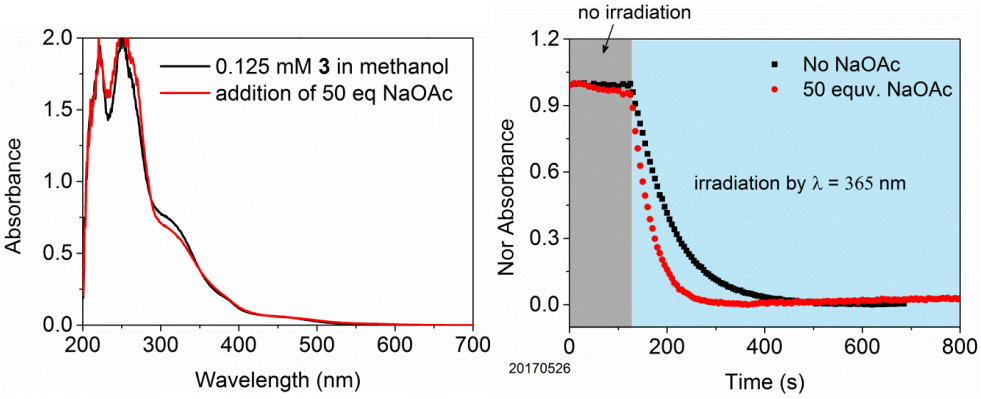

Figure 50. (Left) UV-vis absorption spectrum of **3** (0.125 mM) in methanol with (red) and without (black) NaOAc (6.25 mM). (Right) Normalized absorbance at 310 nm over time in the dark and under irradiation at 365 nm with (red) and without (black) NaOAc (6.25 mM).

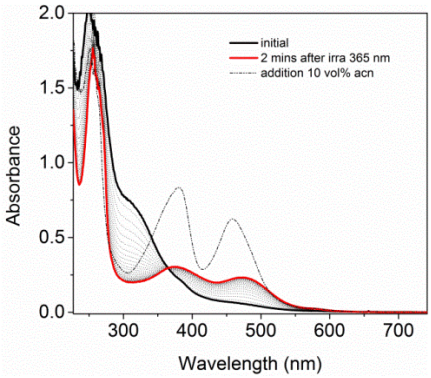

Figure 51. UV-vis absorption spectrum of **2** (0.125 mM) in deoxygenated methanol with NaOAc (6.25 mM), before (black solid line), during (dashed lines) and after (red line) irradiation at 365 nm and after addition of 10 vol % of acetonitrile (dashed black line).

CH_3CN does not significantly displace CH_3O^-, μ-O^{2-} (*see below*) or Cl^-, in the ferric state, as confirmed, for example, by the EPR spectrum of **2**, which shows the characteristic low-spin S = ½ signal (g = 2.28, 2.12, 1.96) for Fe^{III}-OCH_3 (**Figure 52**). Nevertheless, photoreduction of **2, 2a** and **3** was also observed in acetonitrile; however, in contrast to methanol, the initial form of the Fe^{III} complex used played an important role in the observed photochemistry (see below). Furthermore, adventitious water could displace CH_3O^-, μ-O^{2-} or Cl^-, to form $[(L)Fe^{III}\text{-}OH]^{2+}$, as manifested in weaker signals, g = 2.36, 2.16, and 1.94 (**Figure 52**).

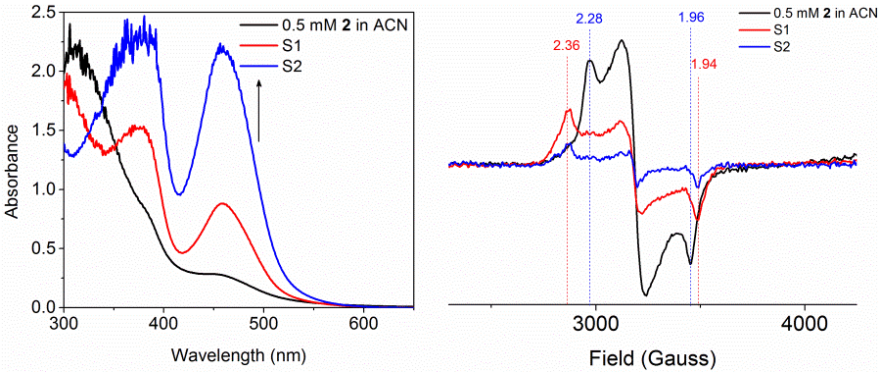

Figure 52. (Left) UV-vis absorption spectrum of **2** (0.5 mM) in acetonitrile before (black), during (red) and after (blue) irradiation at 365 nm. (Right) X-band EPR spectra of corresponding samples rapidly frozen in liquid nitrogen (77 K). g = 2.28, 2.12, 1.96 are the characteristic signals of $[(MeN4Py)Fe^{III}(OCH_3)]^{2+}$ (**2**) and at g = 2.36, 2.16, 1.94 of $[(MeN4Py)Fe^{III}\text{-}OH]^{2+}$.

The photo-reduction of **2** in acetonitrile was orders of magnitude slower than in methanol (**Figure 53**), with a k_{obs} value (from fitting of the change in the absorbance at 310 nm as an exponential decay) of 0.15 s^{-1} in methanol and 0.0066 s^{-1} in acetonitrile (with the same incident light flux). The addition of H_2O (2 vol %, **Figure 54**) or triflic acid (1.0, 5.0, or 50 equiv; **Figure 54**) to **2** in acetonitrile resulted in a substantial decrease in the rate of photoreduction.

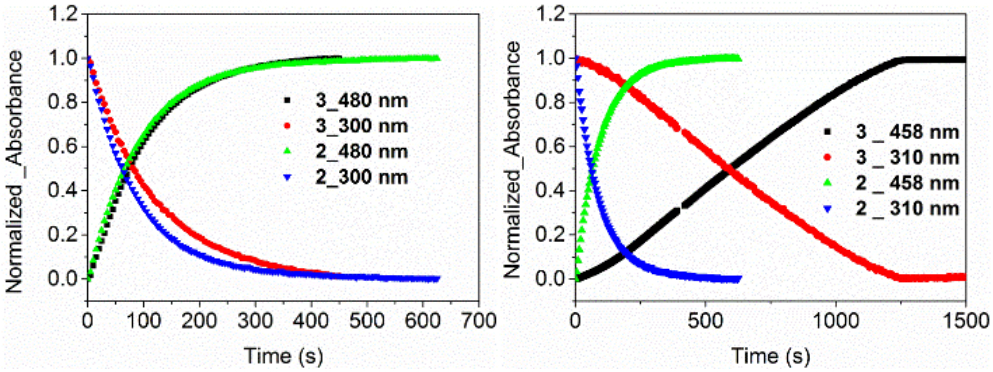

Figure 53. Absorbance of **2** and **3** (0.125 mM) in argon-purged methanol (left; at 300 and 480 nm) and acetonitrile (right; at 310 and 458 nm) during irradiation (λ_{exc} = 365 nm). The initial absorbance at 300/310 and final absorbance at 458/480 nm were used for normalization.

Irradiation of **3** at 365 nm in acetonitrile resulted in an almost linear decrease and increase in absorbance at 310 nm and 480 nm, respectively, due to formation of **1**, and was again much slower than observed in methanol (**Figure 53**). The lower rate is due to the stronger binding of the chlorido ligand of **3**, and hence a reduced extent of exchange with adventitious water to form aqua and dinuclear complexes, such as **2a**. This conclusion was confirmed by the addition of chloride to **2** in acetonitrile, which resulted in a lower rate of reduction. The observed rate is

dependent on irradiation power, thus confirming photokinetic control (**Figure 55**) and the linear decay indicates that the photoreactive species maintains a steady-state concentration throughout most of the reaction.

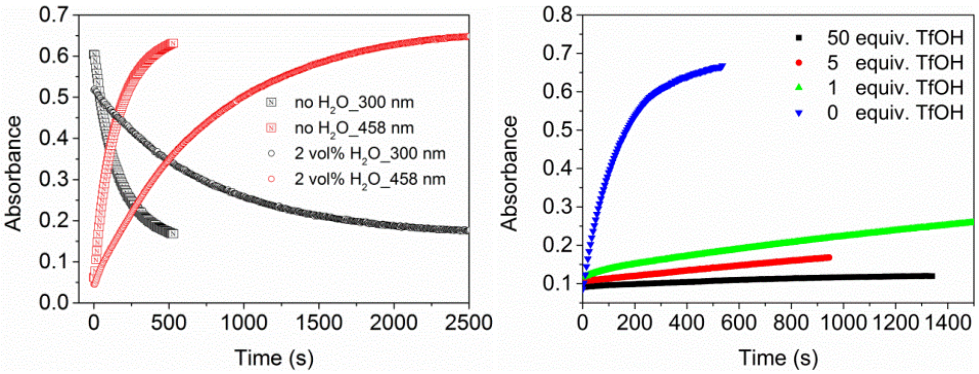

Figure 54. (left) Absorbance at 300 and 458 nm of **2** in deoxygenated acetonitrile under irradiation (λ_{exc} = 365 nm) in the absence and presence of 2 vol% H_2O (v/v). (right) Absorbance at 458 nm of **2** (0.125 mM) in deoxygenated acetonitrile over time under irradiation at 365 nm with 0 (blue), 1 (green), 5 (red) and 50 (black) equiv triflic acid.

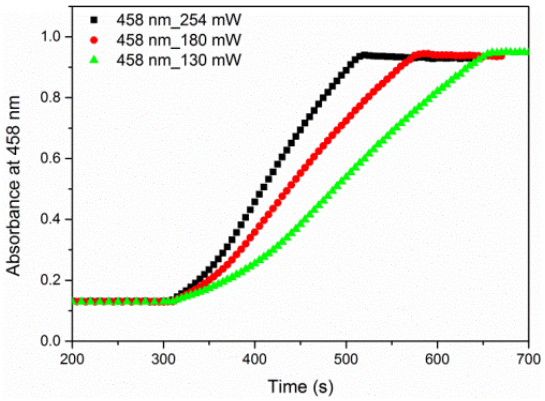

Figure 55. Absorbance at 458 nm over time under irradiation at 365 nm (from 300 s) of **3** in deoxygenated acetonitrile (130 mW – 254 mW).

The ^{1}H-NMR spectrum of **2a** in CD_3CN (**Figure 56**) is similar to that reported for its N4Py analogue[29] and shows moderate paramagnetic line broadening and shift, which is consistent with strong antiferromagnetic coupling of the Fe^{III} centers, and also further confirmed by the absence of signals in its EPR spectrum at 77 K (**Figure 57**). The UV-vis absorption spectrum of **2a** in anhydrous acetonitrile shows the strong absorption at 312 nm (**Figure 48**), which has been assigned to oxo → Fe charge-transfer band,[30] with symmetric and asymmetric bands of a near-linear Fe-O-Fe core[31] at 407 and 810 cm^{-1} , respectively, observed in its resonance Raman (λ_{exc} = 355 nm) spectrum (**Figure 58**). The data confirm that the complex retains its dinuclear structure in anhydrous acetonitrile, in contrast to the equilibration with mononuclear complexes observed in methanol (see above).

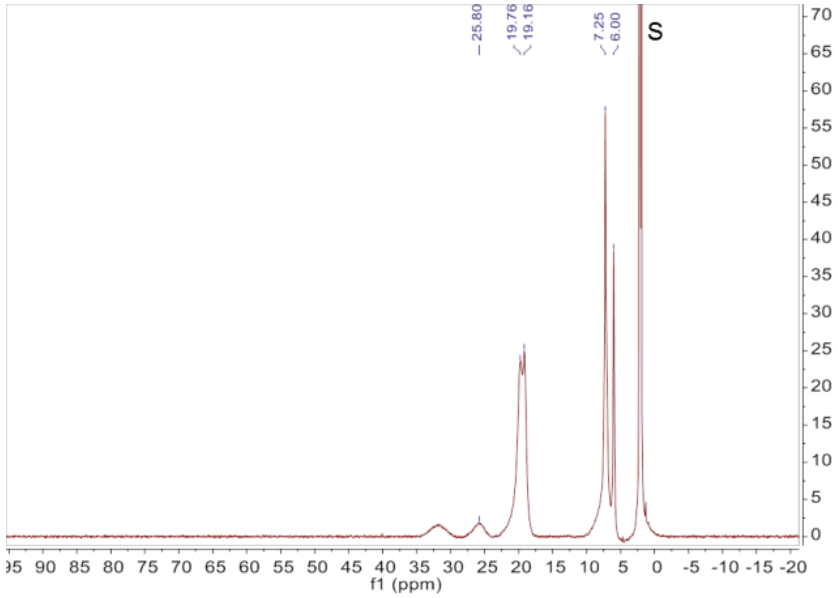

Figure 56. ^{1}H-NMR spectrum of [(MeN4Py)Fe^{III}-μ-O-Fe^{III}(MeN4Py)]$^{4+}$ (**2a**) in CD_3CN, solvent (S) was labelled.

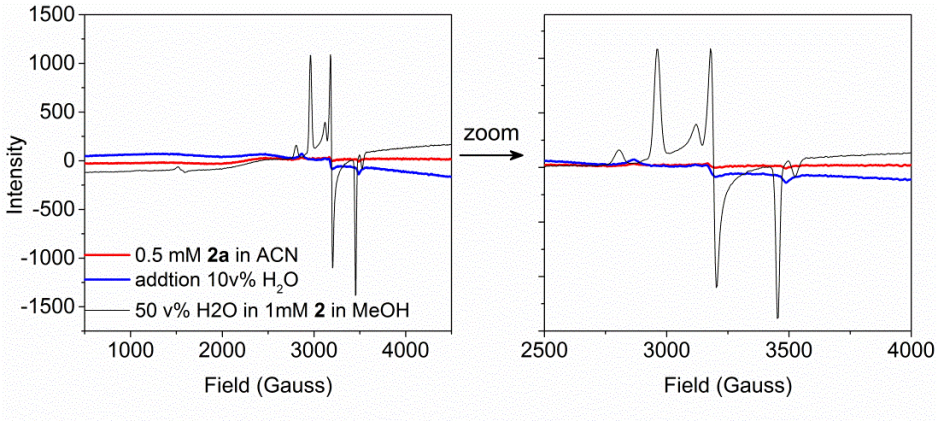

Figure 57. (left) X-band EPR spectra of **2a** (0.5 mM) in anhydrous acetonitrile (red) in liquid nitrogen (77 K); after addition of H_2O (10 vol% ; blue), and EPR spectrum of the 1 mM monomer iron(III) (black). (right) the expansion in region 2500 – 4000 Gauss..

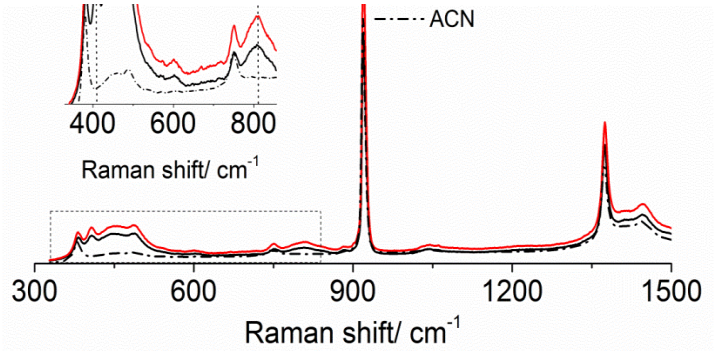

Figure 58. Resonance Raman (λ_{exc} = 355 nm) spectrum of **2a** (0.5 mM) in acetonitrile, before and after addition of H_2O (10 vol%).

Irradiation of **2a** in anhydrous acetonitrile resulted in an increase in the absorbance at 458 nm owing to formation of the Fe^{II} complex (**1**). At higher concentrations, that is, 0.5 mM, an absorption band at 686 nm, characteristic of $[(L)Fe^{IV}=O]^{2+}$ (**4**) appears also (**Figure 59** and **Figure 60**). The addition of excess H_2O to **2a** in acetonitrile had a minor effect on the resonance Raman and EPR spectra (**Figure 57**and **Figure 58**, respectively), thus indicating that the dinuclear structure is largely retained, but accelerated the rate and extent of increase in absorbance at 686 nm (**Figure 59** and **Figure 61**). The subsequent decrease in absorbance at 686 nm after 300 s is due to the photochemical reduction of $[(L)Fe^{IV}=O]^{2+}$ formed.[25] The absence of $[(L)Fe^{IV}=O]^{2+}$ under irradiation of **2a** at lower concentrations in acetonitrile (**Figure 60**) or in methanol (**Figure 45**) is expected considering its low molar absorptivity (400 M^{-1} cm^{-1}) and its own photoreactivity.[25] At higher concentrations of **2a** in acetonitrile, at which the absorbance at 365 nm is above 2, the inner-filter effect allows only partial penetration of light into the solution and the buildup of a significant steady-state concentration of **4** within the bulk.

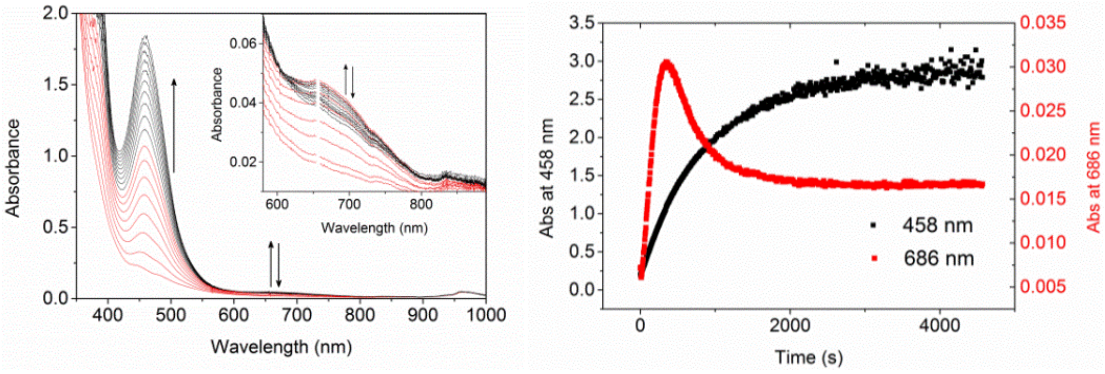

Figure 59. (left) UV-vis absorption spectrum of **2a** (0.5 mM) in acetonitrile with H_2O (10 vol%) during the first 1000 s of irradiation (365 nm); (right) Absorbance at 458 (left y-axis) and 686 nm (right y-axis) over time during irradiation.

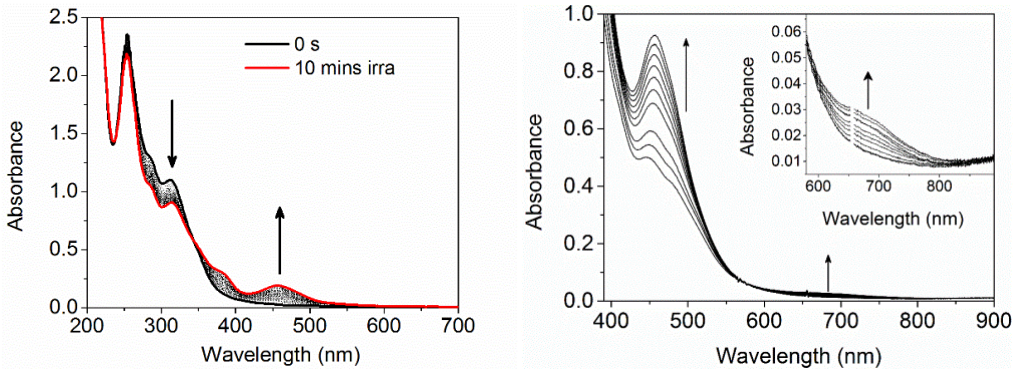

Figure 60. UV-vis spectrum changes under irradiation (365 nm) of **2a** (left: 0.0625 mM; right: 0.5 mM) in anhydrous acetonitrile.

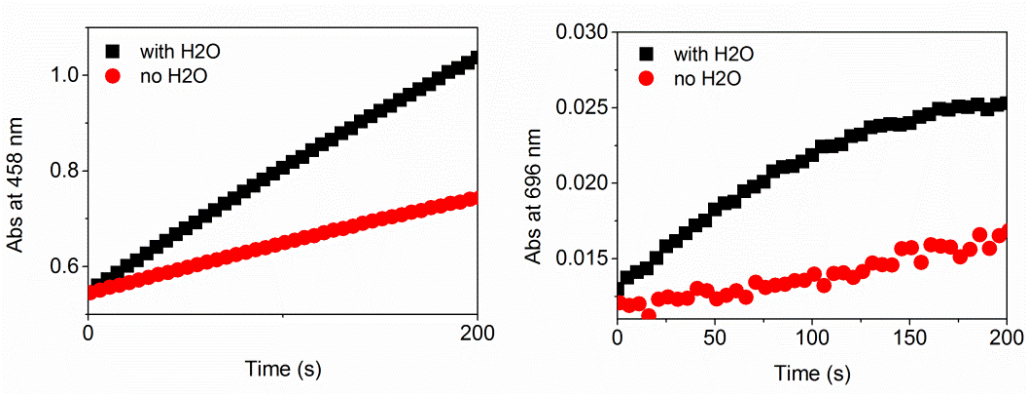

Figure 61. Comparison of the corresponding absorbance changes at 458 and 686 nm of **2a** in acetonitrile under irradiation with and without present of 10 vol % H_2O.

In summary, non-heme iron(III) complexes **2**, **2a** and **3** equilibrate rapidly with argon-purged methanol and show identical photochemical reduction to the Fe^{II} state without ligand degradation. Both EPR spectroscopy and the wavelength dependence of Φ indicate that there are several species present in solution, not all of which are photochemically reactive. In non-heme systems, the equilibrium between mononuclear and μ-oxido-bridged dinuclear Fe^{III} complexes with pentadentate ligands (N4Py, P2DA, **6**-OC_6H_4-TPA, etc.,)[29,32,33] has been shown earlier to be rapid. Addition of base (NaOAc) and proton sources (H_2O or TfOH) shifts the equilibrium towards complexes, such as the mononuclear Fe^{III}-OH, Fe^{III}-OH_2 and the dinuclear Fe^{III}-O-Fe^{III} complexes. In the present reaction, conditions which favor dimer formation (base addition) is accompanied by an increase in the rate of photoreduction, while added proton source or chloride favor formation of mononuclear Fe^{III} complexes and retard photoreduction. A possible mechanism for the photoreduction is shown in **Scheme 6**.

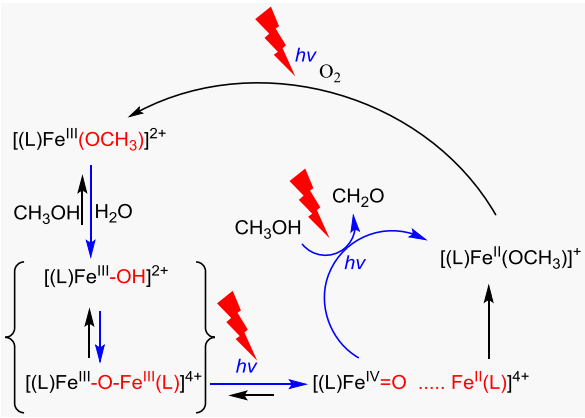

Scheme 6. Overall scheme for the catalytic oxidation of methanol under irradiation.

Photoinduced heterolysis was reported first by Richman and co-workers. In the case of the μ-oxido-bridged diiron(III) porphyrin complexes, visible irradiation resulted in reduction of both Fe^{III} centers to the Fe^{II} redox state via an intermediate Fe^{IV}/Fe^{II} species[34] in the presence of oxidizable substrates;[21,22] reoxidation of the dinuclear Fe^{II} complex was not spontaneous, thus limiting potential for catalytic turnover. In the absence of substrates with weak C-H bonds, the quantum yield for the reduction was negligible due to rapid recombination of the Fe^{IV}=O/Fe^{II} centers to the Fe^{III}-O-Fe^{III} state. Karlin and co-workers[23] have shown that photocatalytic oxidation and aromatic dehalogenation are possible with turnover by using a nonsymmetric dinuclear Fe^{III} complex based on a non-heme Fe^{III} unit and an Fe^{III}-porphyrin, which were bridged by both a μ-oxido unit and a

covalent link between the heme and non-heme ligands. As in the double Fe^{III}-porphyrin systems,[34] an intermediate Fe^{IV}=O/Fe^{II} species was observed by flash photolysis. The Fe^{IV}=O/Fe^{II} species was sufficiently long-lived to react with organic substrates with relatively strong C-H bonds and the Fe^{III}-μ-O-Fe^{III} complex was recovered subsequently by aerobic oxidation. The formation of tetranuclear complexes bearing an inert non-heme Fe^{III}-μ-O-Fe^{III} unit was observed especially in dechlorination reactions.

For heme cofacial porphyrin μ-oxido bridged diiron(III) complexes, irradiation into the oxido → Fe^{III} charge-transfer band[35] results in the photoinduced disproportionation to Fe^{II} and Fe^{IV}=O monomers.[21,22,34] In the present non-heme system, an analogous model would see an Fe^{IV}=O species formed upon excitation of **2a** in methanol or acetonitrile, which can recombine with the Fe^{II} fragment to reform **2a** or react with methanol to form methanal and a second equivalent of an Fe^{II} complex. The electronic nature of the photoreaction and the thermodynamic energies of possible dissociation products were explored by DFT methods and the discussion of these studies can be found in the supporting information of the published paper (*10.1002/anie.201712678*).

The oxidation of $[(MeN4Py)Fe^{II}(CH_3CN)]^{2+}$ (**1**) in methanol to its Fe^{III} state (i.e., **2**) with O_2 as terminal oxidant was reported by our group earlier with visible and UV light.[24] In the present study, we have shown that the iron(III) complexes of the ligand N4Py undergo reduction upon irradiation in methanol. This observation prompted us to explore whether both reactions could proceed under the same conditions simultaneously and thereby enable the catalytic use of O_2 as a terminal oxidant. Irradiation of $[(MeN4Py)Fe^{II}(CH_3CN)]^{2+}$ (**1**) at 365 nm in methanol at room temperature under aerobic conditions resulted in the steady increase in the amount of formaldehyde formed over time (**Scheme 6** and **Figure 62**) with a relatively minor decrease in visible absorbance (33% after 3 h irradiation, **Figure 62**). Over 50 turnovers were observed with respect to **1, thus** confirming that the process is catalytic.

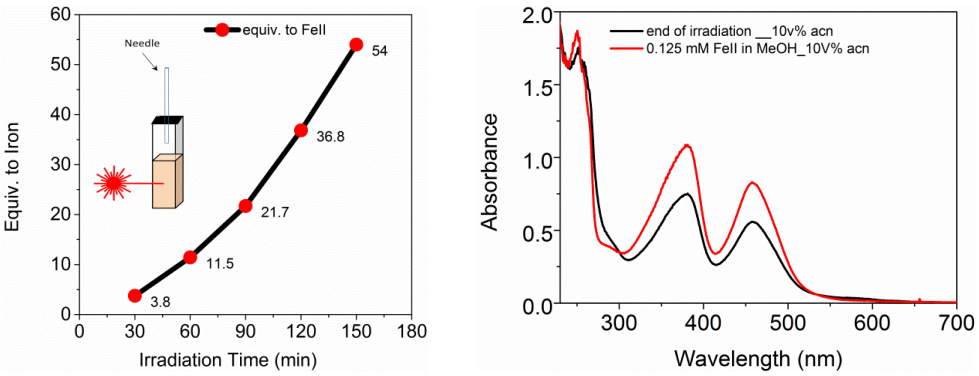

Figure 62. (Left) Formaldehyde formation over time under irradiation in aerated conditions with **1** (0.125 M) in methanol. (right) UV-vis absorption spectrum of **1** (0.125 mM) in methanol after 3 h irradiation under aerobic conditions and after addition of acetonitrile (10 vol%; red).

3.3 Conclusion

In summary, the photoreduction of non-heme Fe^{III} complexes proceeds via an intermediate formed from the mononuclear complexes **2** and **3** or the μ-oxido-bridged diiron(III) complex **2a**. DFT calculations indicate that photoexcitation of **2a** would result in population of antibonding orbitals and drive heterolytic cleavage to form a five-coordinate Fe^{II} species and an Fe^{IV}=O species in an excited electronic state (HS) rather than in its intermediate-spin (IS) ground state. Recombination to reform **2a** competes with solvent coordination (e.g., in acetonitrile to form **1**)

and oxidation of solvent (e.g., methanol to methanal) by the Fe^{IV}=O species formed. This mechanism is analogous to those proposed for the heme Fe^{III} systems reported earlier. Importantly, we show that the present system can use light to achieve a full catalytic cycle in methanol without the need for a secondary photosensitizer. In the presence of O_2, the Fe^{II} species formed undergoes light-driven oxidation by O_2 to close a full photocatalytic cycle with a single catalyst, and oxidation of methanol with O_2 with high turnover numbers. The present system opens opportunities for selective photocatalytic reactions with a single catalyst.

3.4 Experimental section

1,1-di(pyridin-2-yl)-N,N-bis(pyridin-2-ylmethyl)ethan-1-amine(MeN4Py),[28] $[(N4Py)Fe^{II}(CH_3CN)](ClO_4)_2$ (**1**),[29] and $[(MeN4Py)Fe^{III}(OCH_3)](ClO_4)_2$ (**2**),[28] were prepared by previously reported procedures. Commercially available chemicals were purchased from Sigma Aldrich without further purification. All solvents used for spectroscopy were of UVASOL (Merck) grade. $[(MeN4Py)Fe^{III}(Cl)](ClO_4)_2$ (**3**) was prepared by mixing equimolar amounts of $Fe^{III}Cl_3$ and the ligand (MeN4py) in acetonitrile, followed by addition of 10 equiv $NaClO_4$ in a minimum amount of acetonitrile. Vapour diffusion of diethyl ether into the solution at room temperature provided signal crystals of $[(MeN4Py)Fe^{III}(Cl)](ClO_4)_2$. Complex $[(MeN4Py)Fe^{III}\text{-}O\text{-}Fe^{III}(MeN4Py)](ClO_4)_4$ (**2a**) was obtained by slow evaporation of a concentrated solution of $[(MeN4Py)Fe^{III}(Cl)](Cl)_2$[36] in water with added $LiClO_4$.

A single crystal of compound **3** was mounted on top of a cryoloop and transferred into the cold nitrogen stream (100 K) of a Bruker-AXS D8 Venture diffractometer. Data collection and reduction was done using the Bruker software suite APEX3.[37] The final unit cell was obtained from the xyz centroids of 9752 reflections after integration. A multiscan absorption correction was applied, based on the intensities of symmetry-related reflections measured at different angular settings (SADABS). The structures were solved by direct methods using SHELXS, and refinement of the structure was performed using SHLELXL. The hydrogen atoms were generated by geometrical considerations, constrained to idealized geometries and allowed to ride on their carrier atoms with an isotropic displacement parameter related to the equivalent displacement parameter of their carrier atoms. The structure was refined as a two-component inversion twin.

3.5 Acknowledgements

We thank Dr. Stepan Stepanovic for the help with DFT calculations. The COST association action CM1305 ECOSTBio (STSM grant 38503), the European Research Council (ERC 279549, WRB), Labex ARCANE (ANR-11-LABX-003), the Serbian Ministry of Science (OI172035), and the Chinese Scholarship Council (CSC) are acknowledged for financial support. We thank the Center for Information Technology of the University of Groningen for their support and for providing access to the Peregrine high-performance computing cluster. We thank Prof. Edwin Otten for X-ray structural analysis of **3**, and Dr. Carole Duboc and Dr. Sandeep Padamati for recording X-band EPR spectra of **3** at 4 K.

3.6 References

(1) Prier, C. K.; Rankic, D. A.; MacMillan, D. W. C. *Chem. Rev.* **2013**, *113* (7), 5322–5363.

(2) Yoon, T. P.; Ischay, M. A.; Du, J. *Nat. Chem.* **2010**, *2* (7), 527–532.

(3) Ooyama, Y.; Harima, Y. *European J. Org. Chem.* **2009**, *2009* (18), 2903–2934.

(4) Hoffmann, M. R.; Martin, S.; Choi, W.; Bahnemann, D. W. *Chem. Rev.* **1995**, *95* (1), 69–96.

(5) Steel, P. J.; Constable, E. C. *J. Chem. Soc., Dalton Trans.* 1990, *0*, 1389–1396.
(6) Roundhill, D. M. *Photochemistry and Photophysics of Metal Complexes*; Springer US, 1994.
(7) Hoffmann, N. *ChemSusChem* 2012, *5* (2), 352–371.
(8) Adamson, A. W.; Waltz, W. L.; Zinato, E.; Watts, D. W.; Fleischauer, P. D.; Lindholm, R. D. *Chem. Rev.* 1968, *68* (5), 541–585.
(9) Perutz, R. N.; Procacci, B. *Chem. Rev.* 2016, *116* (15), 8506–8544.
(10) Company, A.; Sabenya, G.; González-Béjar, M.; Gómez, L.; Clémancey, M.; Blondin, G.; Jasniewski, A. J.; Puri, M.; Browne, W. R.; Latour, J.-M.; Que, L.; Costas, M.; Pérez-Prieto, J.; Lloret-Fillol, J. *J. Am. Chem. Soc.* 2014, *136* (12), 4624–4633.
(11) Kotani, H.; Suenobu, T.; Lee, Y.-M.; Nam, W.; Fukuzumi, S. *J. Am. Chem. Soc.* 2011, *133* (10), 3249–3251.
(12) DeRosa, M. C.; Crutchley, R. J. *Coord. Chem. Rev.* 2002, *233–234* (Supplement C), 351–371.
(13) Ashen-Garry, D.; Selke, M. *Photochem. Photobiol.* 2014, *90* (2), 257–274.
(14) Abdel-Shafi, A. A.; Worrall, D. R.; Ershov, A. Y. *Dalton Trans.* 2004, *0* (1), 30–36.
(15) Hergueta-Bravo, A.; Jiménez-Hernández, M. E.; Montero, F.; Oliveros, E.; Orellana, G. *J. Phys. Chem. B* 2002, *106* (15), 4010–4017.
(16) Whitten, D. G. *Acc. Chem. Res.* 1980, *13* (3), 83–90.
(17) Demas, J. N.; Harris, E. W.; McBride, R. P. *J. Am. Chem. Soc.* 1977, *99* (11), 3547–3551.
(18) Šima, J.; Makáňová, J. *Coord. Chem. Rev.* 1997, *160*, 161–189.
(19) *Proc. R. Soc. London. Ser. A. Math. Phys. Sci.* 1956, *235* (1203), 518–536.
(20) Abrahamson, H. B.; Rezvani, A. B.; Brushmiller, J. G. *Inorganica Chim. Acta* 1994, *226* (1), 117–127.
(21) Richman, R. M.; Peterson, M. W. *J. Am. Chem. Soc.* 1982, *104* (21), 5795–5796.
(22) Peterson, M. W.; Rivers, D. S.; Richman, R. M. *J. Am. Chem. Soc.* 1985, *107* (10), 2907–2915.
(23) Wasser, I. M.; Fry, H. C.; Hoertz, P. G.; Meyer, G. J.; Karlin, K. D. *Inorg. Chem.* 2004, *43* (26), 8272–8281.
(24) Draksharapu, A.; Li, Q.; Roelfes, G.; Browne, W. R. *Dalton Trans.* 2012, *41* (42), 13180–13190.
(25) Chen, J.; Draksharapu, A.; Harvey, E.; Rasheed, W.; Que, L.; Browne, W. R. *Chem. Commun.* 2017, *53* (91), 12357–12360.
(26) Maafi, M.; Maafi, W. *Int. J. Photoenergy* 2015, *2015*, 454895–12.
(27) Maafi, W.; Maafi, M. *Int. J. Pharm.* 2013, *456* (1), 153–164.
(28) Draksharapu, A.; Li, Q.; Logtenberg, H.; van den Berg, T. A.; Meetsma, A.; Killeen, J. S.; Feringa, B. L.; Hage, R.; Roelfes, G.; Browne, W. R. *Inorg. Chem.* 2012, *51* (2), 900–913.
(29) Roelfes, G.; Lubben, M.; Chen, K.; Ho, R. Y. N.; Meetsma, A.; Genseberger, S.; Hermant, R. M.; Hage, R.; Mandai, S. K.; Young Jr., V. G.; Zang, Y.; Kooijman, H.; Spek, A. L.; Que Jr., L.; Feringa, B. L. *Inorg. Chem.* 1999, *38* (8), 1929–1936.
(30) Kurtz, D. M. *Chem. Rev.* 1990, *90* (4), 585–606.
(31) Sanders-Loehr, J.; Wheeler, W. D.; Shiemke, A. K.; Averill, B. A.; Loehr, T. M. *J. Am. Chem. Soc.* 1989, *111* (21), 8084–8093.
(32) Lange, S. J.; Miyake, H.; Que, L. *J. Am. Chem. Soc.* 1999, *121* (26), 6330–6331.
(33) McDonald, A. R.; Guo, Y.; Vu, V. V; Bominaar, E. L.; Münck, E.; Que, L. *Chem. Sci.* 2012, *3* (5), 1680–1693.
(34) Hodgkiss, J. M.; Chang, C. J.; Pistorio, B. J.; Nocera, D. G. *Inorg. Chem.* 2003, *42* (25), 8270–8277.

(35) Czernuszewicz, R. S.; Macor, K. A.; Li, X. Y.; Kincaid, J. R.; Spiro, T. G. *J. Am. Chem. Soc.* 1989, *111* (11), 3860–3869.

(36) Draksharapu, A.; Angelone, D.; Quesne, M. G.; Padamati, S. K.; Gómez, L.; Hage, R.; Costas, M.; Browne, W. R.; de Visser, S. P. *Angew. Chemie Int. Ed.* 2015, *54* (14), 4357–4361.

(37) Bruker, (2016). APEX3 (v2012.4-3), SAINT (Version 8.18C) and SADABS (Version 2012/1). Bruker AXS Inc., Madison, Wisconsin, U. .